# Electronic Coherence and Nonlinear Susceptibilities of Conjugated Polyenes

**Article** *in* Science · November 1994

DOI: 10.1126/science.266.5183.250 · Source: PubMed



**4 authors**, including:

Shaul Mukamel
University of California, Irvine
**938** PUBLICATIONS **29,023** CITATIONS

SEE PROFILE

our measurements of He and Xe), the transition to SL for a pure noble gas bubble is smooth: At low levels of drive, the bubble pulsates but no light is emitted, and as the drive is increased, the bubble smoothly distorts until its amplitude of pulsation is large enough to concentrate the energy to the level required for SL. This observation stands in contrast to the behavior of doped bubbles (air for example) where the transition is abrupt (*1*). For the case of a pure $N_2$ bubble, the dynamical properties are difficult to probe because of its nonsteady behavior (Fig. 5). The properties of this bubble can only be measured in real time without the benefits of long-time averaging. Such measurements find an expansion ratio ($R_m/R_0$) that varies in time between 6 and 10. At low sound field amplitudes (where the $N_2$ bubble does not glow), the pulsations are periodic and in agreement with the Rayleigh-Plesset equations.

The transduction of sound into light is surprisingly efficient: Light from the 2% Xe mixture is comparable to the bulk sound energy dissipated by viscosity in the absence of the bubble. In fact, as the water containing the 2% Xe bubble was cooled to 1°C, the overall intensity increased by a factor greater than 10 to an average power of 0.5 μW. If the flash widths of such a bubble are still bounded by the 100-ps (*5*) characteristic of air, then the peak powers will be greater than 0.15 W (because there are 33,000 flashes per second in this resonator).

From a practical perspective, the sensitivity of SL to gas content and ambient temperature suggests that further substantial improvements in the characteristics of the emitted radiation are possible. Theoretically, the picture of SL being generated by the implosion of a shock wave that is launched by the collapsing bubble is incomplete. Shock dynamics are not affected by small gas impurities. An unidentified physical process (that is sensitive to doping with noble gases) controls the long-time dynamics and the transition to SL. In this regard, the ambient radius remains a key theoretical unknown (for 1% Ar, $R_0$ = 4 μm; but for 2% Xe, $R_0$ = 8 μm; whereas for pure $N_2$, it is nonsteady). The light-emitting mechanism is also strongly dependent on the gas content of the bubble. The spectrum for He is steeper than can be accounted for by thermal Bremsstrahlung from hot gases. Perhaps the high density and small size of the plasma that forms in the imploded bubble need to be accounted for in a theory of the spectrum of SL. A unifying feature of our investigation is that although SL is a sensitive phenomenon, it is nevertheless robust throughout a rich parameter space.

## REFERENCES AND NOTES


1. B. P. Barber, C. C. Wu, R. Löfstedt, P. H. Roberts, S. J. Putterman, *Phys. Rev. Lett.* **72**, 1380 (1994).
2. B. P. Barber and S. J. Putterman, *Nature* **352**, 318 (1991).
3. R. Hiller, S. J. Putterman, B. P. Barber, *Phys. Rev. Lett.* **69**, 1182 (1992).
4. D. F. Gaitan, L. A. Crum, C. C. Church, R. A. Roy, *J. Acoust. Soc. Am.* **91**, 3166 (1992).
5. B. P. Barber, R. Hiller, K. Arisaka, H. Fetterman, S. J. Putterman, *ibid.*, p. 3061.
6. R. Battino, T. Rettich, T. Tominaga, *J. Phys. Chem. Ref. Data* **13**, 563 (1984).
7. R. Battino, M. Banzhof, M. Bogan, E. Wilhelm, *Anal. Chem.* **54**, 806 (1972).
8. R. Löfstedt, B. P. Barber, S. J. Putterman, *Phys. Fluids A* **5**, 2911 (1993).
9. S. L. Garrett, *J. Acoust. Soc. Am.* **88**, 210 (1990).
10. A. B. Pippard, *The Physics of Vibration* (Cambridge Univ. Press, Cambridge, 1989).
11. F. M. Penning and C. C. J. Addink, *Physica* **1**, 1007 (1934).
12. J. M. Meek and J. D. Craggs, Eds., *Electrical Breakdown of Gases* (Wiley, New York, 1978).
13. H. P. Greenspan and A. Nadim, *Phys. Fluids A* **5**, 1065 (1993).
14. C. C. Wu and P. H. Roberts, *Phys. Rev. Lett.* **70**, 3424 (1993).
15. W. C. Moss, J. W. White, R. A. Day, D. B. Clarke, *preprint UCRL-JC-110666* (Lawrence Livermore National Laboratory, Livermore, CA, 1993).
16. B. P. Barber and S. J. Putterman, *Phys. Rev. Lett.* **69**, 3839 (1992).
17. L. D. Landau and E. M. Lifshitz, *Fluid Mechanics* (Pergamon, New York, ed. 2, 1987).
18. A. J. Walton and G. T. Reynolds, *Adv. Phys.* **33**, 595 (1984).


19. We are indebted to R. Löfstedt and K. Suslick for valuable discussions. Research supported by the U.S. Department of Energy Division of Advanced Energy Projects.

21 June 1994; accepted 23 August 1994


# Electronic Coherence and Nonlinear Susceptibilities of Conjugated Polyenes


Shaul Mukamel, Akira Takahashi, Hong Xiang Wang, Guanhua Chen



**A dynamic theory that connects electronic motions and the nonlinear optical response of conjugated polyenes is developed by introducing the concept of electronic normal modes. A useful picture for the mechanism of optical nonlinearities is obtained by identifying the few dominant modes. This quasi-particle electron-hole representation establishes a close analogy with small semiconductor particles (quantum dots) and is very different from the traditional approach based on electronic eigenstates. The effective conjugation length (coherence size), which controls the scaling and saturation of the static third-order susceptibility $\chi^{(3)}$ with the number of double bonds, is related to the coherence of the relative motion of electron-hole pairs created upon optical excitation.**


The mechanism of optical nonlinearities of conjugated polyenes constitutes an open challenge that poses important fundamental as well as practical problems related to the synthesis of new optical materials with large susceptibilities (*1–4*). Questions such as structure-property relations (*5*) and comparison with other molecular, semiconductor, or metallic materials (*6*) have drawn considerable attention. Quantum chemists traditionally calculate susceptibilities by expanding them using the global (many-body) electronic eigenstates, and optical properties are then related to the eigenvalues and to matrix elements of the dipole operator. Physical insight is developed in terms of the nature of the relevant eigenstates, which serve as a convenient link between experiment and theory. Despite the tremendous progress in computational methods, the calculation of the global eigenstates remains a very demanding objective, which restricts such calculations to relatively small systems (*2*, *7*). Finite field methods, which are based on calculating the ground-state energy in the presence of an external field, are much more effective for off-resonant susceptibilities, which are most relevant for device applications (*7*). However, they do not provide the frequency dependence and shed very little light on the mechanism of the optical response.

It has long been recognized that, by virtue of their delocalized electronic states, conjugated polyenes may have very large polarizabilities (*8*). A scaling of the third-order susceptibility $\chi^{(3)} \sim N^b$, where $N$ is the number of carbon atoms and $4 \leq b \leq 6$, was found for short chains. A crossover of the scaling exponent to $b = 1$ is expected, however, for larger sizes, because the existence of a proper thermodynamic limit (that is, the independence of macroscopic properties on system size) requires that $\chi^{(3)}/N$ should saturate and become independent of $N$. This saturation reflects some effective conjugation length. Its origin is puzzling if we approach the problem from the chemists' perspective. Off-resonant susceptibilities de-


Department of Chemistry, University of Rochester, Rochester, NY 14627, USA.

pend on the collective effect of many eigenstates, and thus, it is very difficult to develop physical intuition by considering individual eigenstates. In addition, the molecular orbitals are delocalized irrespective of molecular size, and they provide no clue for such a coherence size. In reality, conformational disorder and imperfect materials can result in a finite conjugation length, but physically we expect that even an ideal infinite chain should have an intrinsic coherence size.

In contrast, conventional treatments of semiconductors are based on a completely different, quasi-particle picture (6, 9). The structure, transport, and optical properties are not discussed in terms of the global eigenstates but rather are treated by using elementary excitations related to electron-hole pairs. This is a more modest approach because it does not attempt to obtain all properties in a single calculation. However, by using this approach it becomes possible to treat much more complex systems than is possible with the molecular "all or nothing" approach. The connection between the quasi-particle and the molecular viewpoints is not obvious, in part because semiconductors are usually treated in momentum ($k$) space, which is most suitable for infinite, translationally invariant systems, whereas chemical intuition is based primarily on real space arguments.

In this report, we propose an approach that combines the quasi-particle semiconductor ideas with the chemical real space representation of chemical bonding. We use this approach to analyze the size scaling and saturation of the off-resonant susceptibility $\chi^{(3)}$ of polyacetylene. Our picture is based on the single electron, reduced density matrix (*10*) that maps the electronic motions onto a set of coupled harmonic oscillators. These electronic normal modes are then used to develop a different type of chemical intuition by relating the electronic charges and motions directly to the optical response, without ever introducing global molecular eigenstates. We argue that, in the same way that normal modes are very effectively used in the description of nuclear vibrations, they can be applied to electronic motions as well.

Our calculation starts with the Pariser-Parr-Pople (PPP) tight-binding Hamiltonian for $\pi$ electrons, which includes short- and long-range Coulomb interactions, and reproduces many important properties of conjugated polyenes (*2*, *11*)

$$H = \sum_{n,m,\sigma} t_{mn}\hat{\rho}^{\sigma}_{nm} + \sum_{n} U\hat{\rho}^{\uparrow}_{nn}\hat{\rho}^{\downarrow}_{nn}$$

$$+ \frac{1}{2}\sum_{n,m,\sigma,\sigma'}^{n\neq m} V_{nm}\hat{\rho}^{\sigma}_{nn}\hat{\rho}^{\sigma'}_{mm}$$

$$+ \sum_{n}\frac{1}{2}K(x_n - \bar{x})^2 - E(t)\hat{P} \qquad (1)$$

In this model, each carbon atom has a single $p$ orbital. We introduce the binary electron operators $\hat{\rho}^{\sigma}_{nm} = \hat{c}^{\dagger}_{m\sigma}\hat{c}_{n\sigma}$, where $\hat{c}^{\dagger}_{n\sigma}$ ($\hat{c}_{n\sigma}$) creates (annihilates) an electron of spin $\sigma$ at the $n$th carbon atom. These operators satisfy the Fermi anticommutation relation

$$[\hat{c}^{\dagger}_{m\sigma},\hat{c}_{n\sigma'}]_{+} = \delta_{mn}\delta_{\sigma\sigma'} \qquad (2)$$

The first term on the right side of Eq. 1 is the Hückel Hamiltonian, where $t_{mn}$ is the hopping integral between the $n$th and the $m$th atoms; $t_{n,n\pm1} = \beta - \beta' x_n$, and otherwise $t_{nm} = 0$; $x_n$ is the deviation of the $n$th bond length from the mean bond length along the chain. In all calculations, we used $\beta = -2.4$ eV, and $\beta' = -3.5$ eV Å$^{-1}$. The second and third terms include electron-electron Coulomb interactions. An on-site Hubbard repulsion is given by $U = U_0/\varepsilon$, and a repulsion between charges on the $n$th and the $m$th atoms is given by the Ohno formula

$$V_{nm} = U[1 + (r_{nm}/a_0)^2]^{-1/2} \qquad (3)$$

where $r_{nm}$ is the distance between atoms $n$ and $m$. $U_0$, set equal to 11.13 eV, is the unscreened on-site repulsion, $\varepsilon = 1.5$ is the dielectric constant, and $a_0 = 1.2935$ Å. The fourth term describes the $\sigma$ bonds as a set of harmonic oscillators. $K$ is the spring constant ($K = 30$ eV Å$^{-2}$), and $\bar{x} = 0.14$ Å represents the difference in the mean bond length with and without the $\pi$ electrons and controls the average bond length. These parameters reproduce the experimental absorption band edge $E_g$ for polyacetylene ($E_g = 2$ eV). The fifth term represents the dipole interaction between the $\pi$ electrons and a uniform external electric field $E(t)$ polarized along the chain ($z$ direction). The polarization operator is

$$\hat{P} = -q\sum_{n,\sigma} z_n\hat{\rho}^{\sigma}_{nn} \qquad (4)$$

where $-q$ is the electron charge and $z_n$ is the $z$ coordinate of the $n$th atom.

Our approach focuses on the reduced single electron density matrix defined by the expectation value of $\hat{\rho}$

$$\rho_{nm}(t) \equiv \langle\psi(t)|\hat{\rho}^{\sigma}_{nm}|\psi(t)\rangle \qquad (5)$$

with $|\psi(t)\rangle$ being the complete (many-electron) time-dependent wave function. Because both the Hamiltonian and the static Hartree-Fock ground state are symmetric with respect to spin exchange, the wave function must also have this symmetry, and we thus omit the spin index.

The charge density, which is the key quantity in chemical dynamics, is given by the diagonal elements $\rho_{nn}$. The optical polarization can also be calculated with these diagonal elements

$$\langle\hat{P}(t)\rangle = -2q\sum_{n} z_n\rho_{nn}(t) \qquad (6)$$

The off-diagonal elements $\rho_{nm}$ with $n \neq m$ represent spatial coherences. The bond order $p_n$ is related to the off-diagonal nearest neighbor elements $\rho_{n,n\pm1}$ (see discussion below). The density matrix thus provides a compact representation of charge density and bond order that should help establish structure-property relations. The quantity $\rho_{nm}(t)$ represents the coherent and correlated motion of an electron-hole pair created optically, $m$ and $n$ being the electron and hole positions, respectively. By looking directly at the density matrix in real space, we can consider systems with a large number of electrons and study collective electronic motions. The conventional use of the density matrix in nonlinear optics is based on expressing it in terms of the global states of the entire system (*12*). Here, on the other hand, we consider the single particle reduced density matrix in a many-body system that is a completely different object. In metals, electrons and holes are screened and therefore uncorrelated. The elementary excitations (plasmons) are then related to charge density fluctuations (*8*), which can be described by the diagonal elements of the reduced density matrix. By looking at the off-diagonal elements as well, we can define the coherence size and describe correlated particles.

From the Schrödinger equation and the commutation relations for Fermi operators, we obtain a closed equation of motion for the density matrix (*13*)

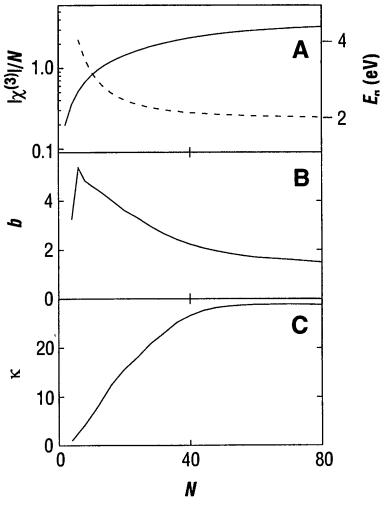


**Fig. 1.** (**A**) Variation of the optical gap $E_g$ (dashed curve) and the static susceptibility $\chi^{(3)}$ in units of $10^{-34}$ electrostatic units (solid curve) with molecular size $N$. (**B**) Variation of the exponent $b = d[\ln \chi^{(3)}]/d[\ln N]$, which controls the scaling of $\chi^{(3)}$ with size, $N$. (**C**) Variation of the inverse participation ratio $\kappa$, which illustrates the coherence length associated with the density matrix, with $N$.

$$i\hbar\dot{\rho}(t) = [\mathbf{h}(t),\rho(t)] \quad (7a)$$

where $\hbar$ is Planck's constant divided by $2\pi$ and $\mathbf{h}(t)$ is the Fock operator matrix of the driven molecule

$$h_{nm}(\rho) = t_{nm} + 2\delta_{nm}\sum_{\ell} V_{n\ell}\rho_{\ell\ell} - V_{nm}\rho_{nm} + \delta_{nm}q\chi_n E(t) \quad (7b)$$

In the derivation of these equations, we have used the time-dependent Hartree-Fock procedure, which assumes that the total wave function can be represented by a single Slater determinant at all times. Equation 7 may be solved in the following steps: First, we decompose $\rho$ as $\rho = \rho^{(0)} + \delta\rho$, where $\rho^{(0)}$ is the density matrix of the Hartree-Fock ground state and $\delta\rho = \rho^{(1)} + \rho^{(2)} + \rho^{(3)} + \ldots$ is induced by the external field where $\rho^{(j)}$ is to $j$th order in the external field. The Fock operator matrix $\mathbf{h}$ is decomposed in the same way. Substituting these quantities into the nonlinear Eq. 7a, we find that $\delta\rho_{nm}$ is coupled to $\delta\rho_{n'm'}$ as well as to bilinear products $\delta\rho_{n'm'}\delta\rho_{n''m''}$. We can then solve the equation successively, order by order, in the external field. In the zeroth-order calculation [$\rho^{(0)}$], we have optimized the geometry by minimizing the energy with respect to $x_n$, which results in bond alternation.

In the following, we analyze the third-order off-resonant electronic susceptibility $\chi^{(3)}$ calculated when the field $E(t)$ has zero frequency. It is obtained by dividing the optical polarization calculated using $\rho^{(3)}$ by $E^3$. Figure 1A shows the variation of the absorption band gap $E_g$ and $\chi^{(3)}$ with size. Both quantities begin to saturate to the infinite size value at about 40 carbon atoms. The nonlinear susceptibility increases by a factor of 670 when the molecular size is increased from 2 to 80 atoms. Figure 1B shows the slope $b$ of this curve [$\chi^{(3)} \sim N^b$]; $b$ reaches a maximum value of $b \approx 5$ at $N = 6$ and then decreases gradually toward the thermodynamic limit $b = 1$.

One can obtain a clear insight by examining some characteristic projections of the single-electron density matrices underlying $\chi^{(3)}$. We define the alternating component of charge density (the diagonal elements of $\rho$)

$$d_n \equiv (-1)^{n-1}(2\rho_{nn} - 1) \quad (8)$$

which measures the magnitude of the charge oscillations, and the alternating component of bond order (the first off-diagonal elements of $\rho$)

$$p_n \equiv (-1)^{n-1}(\rho_{n,n+1} + \rho_{n+1,n} - \bar{p}) \quad (9)$$

where $\bar{p}$ is the average value of $\rho_{n,n+1} + \rho_{n+1,n}$. The quantities $d_n$ and $p_n$ can also be expanded in powers of $E$: These quantities for $\rho^{(j)}$, $j = 0 \ldots 3$, and $N = 80$ are displayed in Fig. 2A. The quantities $\rho^{(1)}$ and $\rho^{(3)}$ are characterized primarily by charge density and have a vanishing bond-order change. We can see charge density wave-like electronic structure in both orders, whereas $\rho^{(0)}$ and $\rho^{(2)}$ are characterized by a bond alternation and no charge density. In the static Hartree-Fock ground state, the bond order is almost uniformly alternated, namely, $p_n^{(0)}$ is almost independent of $n$. In second order, we see that the strength of bond alternation is reduced around the chain center. We thus show $p_n$ for $\rho^{(0)}$ and $\rho^{(2)}$ and $d_n$ for $\rho^{(1)}$ and $\rho^{(3)}$.

A complementary interesting perspective is obtained by considering the "antidiagonal" projection, that is, $\rho_{nm}^{(j)}$ plotted versus $n - m$ with $n + m$ held fixed at $n + m = N + 1$ (Fig. 2B). Note that $\rho_{nm}^{(1)} = 0$ when $n - m$ is even and $n \neq m$. Thus, we show $\rho_{nm}^{(1)}$ where $n - m$ is odd. We find that $\rho_{nm}^{(j)}$ is symmetric in zeroth and second order and is asymmetric in first and third order. Figure 2B shows that $\rho^{(0)}$ is almost diagonal, and $\rho_{nm}^{(0)}$ essentially vanishes for $|n - m| > 3$. The most notable difference among $\rho^{(0)}$, $\rho^{(1)}$, $\rho^{(2)}$, and $\rho^{(3)}$ is the gradual increase in the spread of the off-diagonal elements, which is a signature of field-induced spatial coherence of an electron-hole pair. The extent of this spread, that is, the number of sites that $\rho_{nm}^{(3)}$ covers can be effectively described by the inverse participation ratio $\kappa$,

$$\kappa^{-1} = \sum_{n-m} |\rho_{nm}^{(3)}|^2 \quad (10)$$

with

$$\sum_{n-m} |\rho_{nm}^{(3)}|$$

normalized to one, or

$$\sum_{n-m} |\rho_{nm}^{(3)}| = 1$$

In Fig. 1C, we display the variation of $\kappa$ with $N$. The saturation of this curve is a clear signature of the coherence size associated with the electron-hole pair. It correlates nicely with $\chi^{(3)}$ and the gap energy $E_g$. Numerous definitions and criteria have been suggested for the "conjugation length" or "coherence size." In periodic solids, the size of the Wannier functions is often used. The present analysis applies to finite systems and suggests that $\kappa$, which measures the antidiagonal cross section of the density matrix, is the natural microscopic coherence length responsible for $\chi^{(3)}$.

The direct correlation between spatial electronic coherences and $\chi^{(3)}$ can be used to develop a real space physical picture in which the molecule is described as a collection of driven, coupled harmonic oscillators. The response of these oscillators to the external electric field and the anharmonic couplings between them determine the optical properties. The oscillator picture can be established by a consideration of the homogeneous part of Eq. 7a, which is linear in $\delta\rho$ and is independent of the external field. We search for normal modes of the density matrix in the form (*13*)

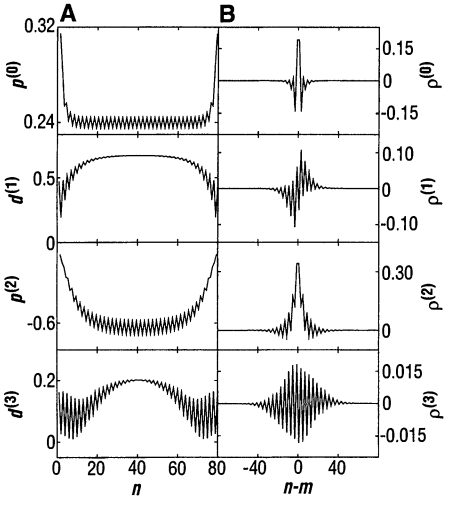


**Fig. 2.** Characteristics of the reduced density matrix of polyacetylene with 80 carbon atoms. The panels from top to bottom correspond to $\rho^{(j)}$, $j = 0, 1, 2, 3$, respectively. (**A**) Charge density $d_n$ for $\rho^{(1)}$ and $\rho^{(3)}$, and bond order $p_n$ for $\rho^{(0)}$ and $\rho^{(2)}$. (**B**) The antidiagonal projections of $\rho_{nm}$ plotted versus $n - m$ with a fixed $n + m = N + 1$. The absolute scale in the vertical axis corresponds to a typical value of the electric field strength $|E| = 1$ V Å$^{-1}$. The curves themselves do not depend on the field strength.

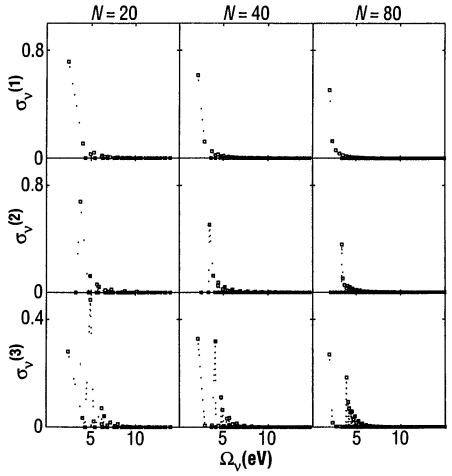


**Fig. 3.** Projections of the density matrix to first, second, and third order in the external field (from top to bottom) on the electronic normal modes for three different molecular sizes. The quantity $\sigma_\nu^{(j)}$ is the component of the $j$th order density matrix corresponding to the $B_u(\nu)$ electronic mode when $j = 1$ or 3 and the $A_g(\nu)$ mode when $j = 2$. The dotted line is a guide to the eye. Note the appearance of a strong $B_u$ mode in $\delta\rho^{(3)}$, which is absent in $\delta\rho^{(1)}$. This contribution is induced by anharmonicities.

$$\psi^{\nu}(t) = \psi^{\nu}\exp(-i\Omega_{\nu}t) \quad (11)$$

where $\Omega_{\nu}$ are the frequencies (eigenvalues). Substituting this into the linearized time-dependent Hartree-Fock equation, we obtain an eigenvalue equation that defines a set of "electronic normal modes," which form a harmonic oscillator basis set. The density matrix can be expanded with these normal modes

$$\delta\rho_{mn}(t) = \sum_{\nu}\delta\rho_{\nu}\psi^{\nu}_{mn} \quad (12)$$

where $\delta\rho_{\nu}$ are the expansion coefficients. The time-dependent Hartree-Fock equation in the harmonic oscillator representation then becomes

$$i\hbar\delta\dot{\rho}_{\nu} - \Omega_{\nu}\delta\rho_{\nu} = F_{\nu} + E\sum_{\nu'}T_{\nu,\nu'}\delta\rho_{\nu'} + \sum_{\nu',\nu''}S_{\nu,\nu'\nu''}\delta\rho_{\nu'}\delta\rho_{\nu''} \quad (13)$$

The first, second, and third terms in the right side of Eq. 13 represent the driving force due to the external field, a nonlinear coupling between the external field and oscillators, and anharmonic couplings among oscillators, respectively. Both the second and third terms describe effects higher than the first order in the external field. This representation provides an invaluable physical insight regarding the origin of $\chi^{(3)}$ because it allows us to think of the polyene as a collection of $N^2/2$ coupled harmonic oscillators. Note that nowhere did we have to introduce the global (many-body) molecular states.

In Fig. 3 we display the normalized expansion coefficients

$$\sigma^{(j)}_{\nu} \equiv |\delta\rho^{(j)}_{\nu}|/\sum_{\nu}|\delta\rho^{(j)}_{\nu}| \quad (14)$$

of the density matrices versus the oscillator frequency $\Omega_{\nu}$ for three molecular sizes, $N$ = 20, 40, and 80. From top to bottom Fig. 3 shows the dominant oscillators in the first-, second-, and third-order response. It is remarkable that there are only three dominant oscillators. Because the molecule has an inversion symmetry, the oscillators can be classified as either symmetric ($A_g$) or antisymmetric ($B_u$). Two of the dominant oscillators have a $B_u$ symmetry, and one has $A_g$ symmetry. In Figs. 4 and 5 we display the characteristics of the density matrices $\psi^{\nu}_{nm}$ of these relevant oscillators. Figure 4 shows the charge density and bond order, whereas Fig. 5 shows the antidiagonal projections. These figures illustrate how the coherence size associated with these oscillators saturates for large sizes. This tendency toward saturation provides the microscopic mechanism for the saturation of $\chi^{(3)}$.

The reduced ground-state, single electron density matrix has been extensively used in the 1960s in the discussion of aromactivity and photochemistry (the Woodward-Hoffman rules) (*11*) but was never pursued for the calculation of optical properties. Density matrices of few-level systems are very successfully used in the interpretation of magnetic resonance and optical spectroscopies of simple chromophores. The present calculation demonstrates the applicability of density matrices as a computational tool, and it provides a direct and simple physical picture of the optical response. The combination of the real space "chemistry" view with the electron-hole "physics" representations offered by off-diagonal elements of the reduced single electron density matrix in real space helps bridge the gap between the physical picture of semiconductor and molecular materials. We obtained electronic normal modes, which represent collective exciton states and treated them in the same fashion as nuclear vibrations.

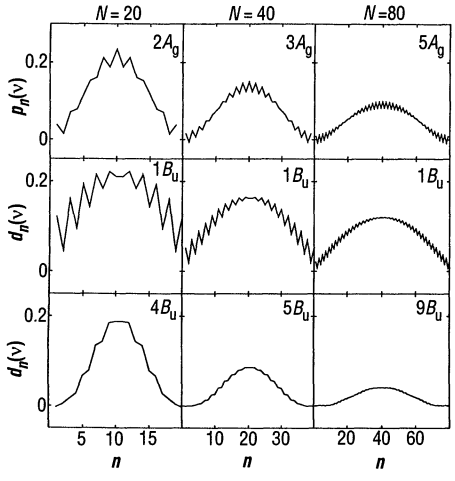


**Fig. 4.** The charge density $d_n(\nu)$ and bond order $p_n(\nu)$ profiles of the three electronic normal modes that dominate the static $\chi^{(3)}$: one $B_u$ [$B_u(1)$] mode for the first order, one $A_g$ mode for the second order, and two $B_u$ [$B_u(1)$ and another $B_u$] modes for the third order. Note the convergence of the dominant normal modes with size.

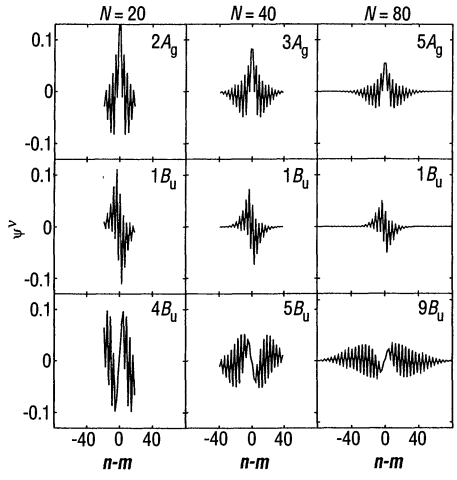


**Fig. 5.** The antidiagonal projections of the three electronic modes shown in Fig. 4. Shown are $\psi^{\nu}_{nm}$ versus $n - m$ with $n + m = N + 1$.

What makes this approach most natural? The conventional quantum chemistry machinery focuses on the independent particle (Hartree-Fock) picture, which is conceptually very attractive. However, optical processes always create pairs of particles (that is, electron-hole pairs) rather than single particles. The density matrix with its two indices keeps track explicitly of the electron and the hole and their correlations. This is why we have $\sim N^2$ rather than $N$ oscillators. It therefore allows us to relate the optical response directly to the molecular structure and to motions of charges, without the tedious intermediate step of calculating the global molecular eigenstates. Because the essential physical picture is built in, this approach works well even when very drastic approximations are made. We pay an initial price for squaring the space size, but this pays off immediately because the number of relevant oscillators is small. A comparable accuracy in the sum over states approach would require a much more elaborate configuration-interaction calculation to make up for the independent particle representation. The applicability of an electronic normal mode harmonic picture to describe nonlinear effects may seem somewhat peculiar at first glance. Strictly speaking, the system is anharmonic (otherwise all nonlinear susceptibilities will vanish identically). However, the anharmonicities are weak and the normal modes provide a convenient picture, in complete analogy with vibrational spectroscopy.

By varying the Coulomb interaction strength $U$ (*14*), we can analyze directly its spectroscopic manifestations. If we switch $U$ off, the density matrix and the electronic normal modes change drastically and the oscillator strength becomes much more uniformly distributed among the various oscillators. The collective nature of electronic motions can therefore be attributed to the Coulomb interaction, which results in the accumulation of oscillator strength in an intense band-edge transition (*13*). By selectively switching off anharmonic coupling terms, we can address separately the roles of Coulomb and exchange interactions in the equations of motion. In the sum over states approach, these are hidden in the wave functions and energies that enter into the multiple summations.

The establishment of structure-property relations can be greatly facilitated with the oscillator approach because it is most natural for describing effects such as substitutions with donors and acceptors, doping, chain dislocations, and so forth. It can also be easily applied to resonant spectroscopies where other cooperative effects are

important. Another important advantage of the oscillator approach over the sum over states approach is that in the latter calculation there are important interferences and cancellations among large terms (*3*). This makes it hard to develop physical intuition, and the computation becomes very sensitive to approximations such as truncation. Also in a sum over states approach, it is impossible to identify beforehand which states will be dominant. The search for the "essential states" is a major difficulty in the modeling of optical nonlinearities. In the oscillator approach, only the relevant oscillators show up in the equations of motion. We thus do not end up calculating a large number of unnecessary quantities.

It should be emphasized that there is no simple one to one correspondence between oscillators and individual eigenstates. The oscillators are collective excitations, and each oscillator represents many states. The precise relation between the two pictures is a highly nontrivial question that needs to be explored further. Symmetry plays a very different role in the eigenstate and in the oscillator representation. In the present model, the Hamiltonian is block diagonal into $A_g$ and $B_u$ symmetry parts, and all of the oscillators may be classified into either $A_g$ or $B_u$ type. In contrast to the description in terms of eigenstates of the Hamiltonian, where $B_u$ and $A_g$ states do not couple at all, $B_u$ and $A_g$ oscillators do couple in the equation of motion (Eq. 13). This fundamental difference between the oscillator and the eigenstate expansions is related to the nonlinear form of the equations of motion (a product of $B_u$ and $A_g$ variables can have a $B_u$ character), as opposed to the eigenstates expansion which are linear. Potentially this allows for a relatively inexpensive method for describing complex physical situations, compared with the expenditure required for eigenstate expansions.

With the current representation, we can use the same language to describe very different materials and answer some of the pressing questions raised recently (*6*). In particular, we can draw a close analogy between conjugated polyenes and semiconductor quantum dots (*9*). The physical picture of geometrically confined electron-hole pairs shows an origin in common with the blue shift of linear absorption as the size is decreased, and with the scaling and saturation of optical nonlinearities.

## REFERENCES AND NOTES


1. J. F. Heflin, K. Y. Wong, Q. Zamani-Khamiri, A. F. Garito, *Phys. Rev. B* **38**, 157 (1988); W. E. Torruellas, D. Neher, R. Zanoni, G. I. Stegeman, F. Kajzar, *Chem. Phys. Lett.* **175**, 11 (1990); M. Cha *et al.*, *ibid.*, in press.
2. S. Etemad and Z. G. Soos, in *Spectroscopy of Advanced Materials*, R. J. H. Clark and R. E. Hester, Eds. (Wiley, New York, 1991), pp. 87–133, and references therein.
3. S. Mukamel, in *Molecular Nonlinear Optics*, J. Zyss, Ed. (Academic Press, New York, 1994), pp. 1–46; *Principles of Nonlinear Optical Spectroscopy* (Oxford, Univ. Press, New York, in press).
4. W. J. Buma, B. E. Kohler, T. A. Schuler, *J. Chem. Phys.* **96**, 399 (1992).
5. S. R. Marder, D. N. Beratan, L.-T. Cheng, *Science* **252**, 103 (1991); S. R. Marder *et al.*, *ibid.* **261**, 186 (1993); S. M. Risser, D. N. Beratan, S. R. Marder, *J. Am. Chem. Soc.* **115**, 7719 (1993).
6. B. I. Greene, J. Orenstein, S. Schmitt-Rink, *Science* **247**, 679 (1990).
7. J. L. Bredas, C. Adant, P. Tackx, A. Persoons, B. M. Pierce, *Chem. Rev.* **94**, 243 (1994).
8. C. Flytzanis and J. Hutter, in *Contemporary Nonlinear Optics*, G. P. Agrawal and R. W. Boyd, Eds. (Academic Press, San Diego, 1992), pp. 297–365.
9. L. Banyai and S. W. Koch, *Semiconductor Quantum Dots* (World Scientific, New York, 1993).
10. P. Fulde, *Electron Correlations in Molecules and Solids* (Springer, New York, 1993).
11. H. Fukutome, *J. Mol. Struct. (Theochem.)* **188**, 337 (1989), and references therein.
12. N. Bloembergen, *Nonlinear Optics* (Benjamin, New York, 1965).
13. A. Takahashi and S. Mukamel, *J. Chem. Phys.* **100**, 2366 (1994).
14. I. Ohmine, M. Karplus, K. Schulten, *ibid.* **68**, 2298 (1978).


15. This research was supported by the Air Force Office of Scientific Research, The National Science Foundation (NSF), and the NSF Center for Photoinduced Charge Transfer.

1 June 1994; accepted 17 August 1994


# Simulating the Self-Assembly of Gemini (Dimeric) Surfactants


S. Karaborni,* K. Esselink, P. A. J. Hilbers, B. Smit, J. Karthäuser, N. M. van Os, R. Zana



**The morphologies and dynamics of aggregates formed by surfactant molecules are known to influence strongly performance properties spanning biology, household cleaning, and soil cleanup. Molecular dynamics simulations were used to investigate the morphology and dynamics of a class of surfactants, the gemini or dimeric surfactants, that are of potential importance in several industrial applications. Simulation results show that these surfactants form structures and have dynamic properties that are drastically different from those of single-chain surfactants. At the same weight fraction, single-chain surfactants form spherical micelles whereas gemini surfactants, whose two head groups are coupled by a short hydrophobic spacer, form thread-like micelles. Simulations at different surfactant concentrations indicate the formation of various structures, suggesting an alternative explanation for the unexpected viscosity behavior of gemini surfactants.**


It is well known that surfactant molecules, which contain a hydrophobic chain and a hydrophilic head group, can form a variety of aggregates with properties different from those of the unassembled molecules. Indeed, spherical micelles, rod-like micelles, bilayers, reverse micelles, and vesicles have all been observed. This polymorphism forms the basis of many biochemical processes and is used in many industrial and household applications. A detailed understanding of surfactant self-assembly is therefore important in processes ranging from the transport of molecules through a cell membrane to the removal of stains in a washing machine (*1*).

In 1974, a class of surfactants was synthesized; these surfactants have two hydrophobic chains and two hydrophilic head groups connected with a spacer (*2*). These surfactants, which were later termed gemini (*3*) or dimeric surfactants (*4*), have unusual characteristics, such as a very low critical micelle concentration and a high efficiency in reducing the oil-water interfacial tension in comparison with conventional single-chain surfactants. These properties suggest that gemini may be excellent surfactants for soil cleanup and enhanced oil recovery; gemini are also possible candidates for the next generation of surfactants (*5*).

In a mixture of water and single-chain surfactants, the system tries to minimize its free energy by forming micelles in which the hydrophobic chains are brought together to minimize the contact with water. The hydrophilic head groups are kept near the water and away from each other as a result of electrostatic repulsions. In a gemini surfactant the two head groups are chemically linked by a hydrophobic spacer; as a consequence, a compromise has to be found for the location of the spacer depending on its length and flexibility and on the degree of repulsion between the two similarly charged head groups. For example, when the spacer length is shorter than the equilibrium distance between two charged head groups, the spacer will be fully extended to minimize the repulsion between the head groups. This positioning leads to a large unfavorable contact


S. Karaborni, K. Esselink, P. A. J. Hilbers, B. Smit, J. Karthäuser, N. M. van Os, Shell Research B.V., Koninklijke/Shell-Laboratorium, Amsterdam, Post Office Box 38000, 1030 BN Amsterdam, Netherlands.
R. Zana, Institut Charles Sadron, Centre National de la Recherche Scientifique, 6 rue Boussingault, 67083 Strasbourg Cedex, France.

*To whom correspondence should be addressed.